Journal of Turbomachinery Published by ASME
Dear Author,

Congratulations on having your paper accepted for publication in the ASME Journal Program.
Your page proof is available in PDF format from the ASME Proof Download & Corrections site here:
http://115.111.50.156/jw/AuthorProofLogin.aspx?pwd=d3a22f63f64d

Login: your e-mail address
Password: d3a22f63f64d

Please keep this email in case you need to refer back to it in the future.
You will need Adobe Acrobat Reader software to view the file. This is free software and a download link is provided when you log in to view your proofs.

Responsibility of detecting errors rests with the author. Please review the page proofs carefully and:

1. Answer any queries on the first page “Author Query Form”
2. Proofread any tables and equations carefully
3. Check to see that any special characters have translated correctly
4. Publication will not proceed until a response is received. If there are no corrections, a response is still required.

RETURNING CORRECTIONS:
Corrections must be returned using the ASME Proof Download & Corrections Submission Site (link above). You will be able to upload:

1. Annotated PDF
2. Text entry of corrections, with line numbers, in the text box provided
3. Additional files, if necessary.

SPECIAL NOTES:
Your Login and Password are valid for a limited time. Please reply within 48 hours.

Corrections not returned through the above website will be subject to publication delays.
This e-proof is to be used only for the purpose of returning corrections to the publisher.
If you have any questions, please contact: asme.cenveo@cenveo.com, and include your article no. (TURBO-14-1159) in the subject line. This email should not be used to return corrections.

Sincerely,
Mary O'Brien, Journal Production Manager

STATEMENT OF EDITORIAL POLICY AND PRACTICE

The Technical Committee on Publications and Communications (TCPC) of ASME aims to maintain a high degree of technical, literary, and typographical excellence in its publications. Primary consideration in conducting the publications is therefore given to the interests of the reader and to safeguarding the prestige of the Society.

To this end the TCPC confidently expects that sponsor groups will subject every paper recommended by them for publication to careful and critical review for the purpose of eliminating and correcting errors and suggesting ways in which the paper may be improved as to clarity and conciseness of expression, accuracy of statement, and omission of unnecessary and irrelevant material. The primary responsibility for the technical quality of the papers rests with the sponsor groups.

In approving a paper for publication, however, the TCPC reserves the right to submit it for further review to competent critics of its own choosing if it feels that this additional precaution is desirable. The TCPC also reserves the right to request revision or condensation of a paper by the author or by the staff for approval by the author. It reserves the right, and charges the editorial staff, to eliminate or modify statements in the paper that appear to be not in good taste and hence likely to offend readers (such as obvious advertising of commercial ventures and products, comments on the intentions, character, or acts of persons and organizations that may be construed as offensive or libelous), and to suggest to authors rephrasing of sentences where this will be in the interest of clarity. Such rephrasing is kept to a minimum.

Inasmuch as specific criteria for the judging of individual cases cannot, in the opinion of the TCPC, be set up in any but the most general rules, the TCPC relies upon the editorial staff to exercise its judgment in making changes in manuscripts, in rearranging and condensing papers, and in making suggestions to authors. The TCPC realizes that the opinions of author and editor may sometimes differ, and hence it is an invariable practice that no paper is published until it has been passed on by the author. For this purpose page proofs of the edited paper are sent to the author prior to publication in a journal. Changes in content and form made in the proofs by authors are followed by the editor except in cases in which the Society's standard spelling and abbreviation forms are affected.

If important differences of opinion arise between author and editor, the points at issue are discussed in correspondence or interview, and if a solution satisfactory to both author and editor is not reached, the matter is laid before the TCPC for adjustment.

Technical Committee on Publications and Communications (TCPC)
Reviewed: 05/2012

AUTHOR QUERY FORM

ASME SETTING THE STANDARD	**Journal: J. Turbomach.** **Article Number: TURBO-14-1159**	**Please provide your responses and any corrections by annotating this PDF and uploading it to ASME's eProof website as detailed in the Welcome email.**

Dear Author,

Below are the queries associated with your article; please answer all of these queries before sending the proof back to Cenveo. Production and publication of your paper will continue after you return corrections or respond that there are no additional corrections.

Location in article	Query / Remark: click on the Q link to navigate to the appropriate spot in the proof. There, insert your comments as a PDF annotation.
AQ1	Standard journal style does not allow the use of the acronyms in the title; therefore, we have replaced the acronym CFD with the spelled out definition.
AQ2	Please provide postal codes/zip codes for all affiliations.
AQ3	Please note that Ref. [23] is changed to [22] to match with the authors cited in the text. Please check and confirm.
AQ4	Please note that Appendix Figure A1 has been changed to Fig. 13 to follow sequential numbering from the body of the paper. Please check and confirm.
AQ5	Please provide report number in Refs. 1 and 23.
AQ6	Please provide date of conference held and page number in Refs. 2, 6, and 31.
AQ7	Please provide more information in Refs. 7 and 21.
AQ8	Please note that references should be cited sequentially in text. Hence we have renumbered the reference citation and reference list in sequential order. Please check and confirm.
AQ9	Please provide issue number for Refs. 9.

Thank you for your assistance.

Quantitative Computational Fluid Dynamics Analyses of Particle Deposition on a Transonic Axial Compressor Blade—Part I: Particle Zones Impact

Alessio Suman
Dipartimento di Ingegneria,
Università degli Studi di Ferrara,
Ferrara ■, Italy

Rainer Kurz
Solar Turbines Incorporated,
San Diego, CA ■

Nicola Aldi
Dipartimento di Ingegneria,
Università degli Studi di Ferrara,
Ferrara ■, Italy

Mirko Morini
Dipartimento di Ingegneria Industriale,
Università degli Studi di Parma,
Parma ■, Italy

Klaus Brun
Southwest Research Institute,
San Antonio, TX ■

Michele Pinelli
Dipartimento di Ingegneria,
Università degli Studi di Ferrara,
Ferrara ■, Italy

Pier Ruggero Spina
Dipartimento di Ingegneria,
Università degli Studi di Ferrara,
Ferrara ■, Italy

Solid particle ingestion is one of the principal degradation mechanisms in the turbine and compressor sections of gas turbines. In particular, in industrial applications, the microparticles that are not captured by the air filtration system cause fouling and, consequently, a performance drop of the compressor. This paper presents three-dimensional numerical simulations of the microparticle ingestion (0 μm–2 μm) on an axial compressor rotor carried out by means of a commercial computational fluid dynamic (CFD) code. Particles of this size can follow the main air flow with relatively little slip, while being impacted by flow turbulence. It is of great interest to the industry to determine which areas of the compressor airfoils are impacted by these small particles. Particle trajectory simulations use a stochastic Lagrangian tracking method that solves the equations of motion separate from the continuous phase. Then, the NASA Rotor 37 is considered as a case study for the numerical investigation. The compressor rotor numerical model and the discrete phase treatment have been validated against the experimental and numerical data available in literature. The number of particles, sizes, and concentrations are specified in order to perform a quantitative analysis of the particle impact on the blade surface. The results show that microparticles tend to follow the flow by impacting at full span with a higher impact concentration on the pressure side (PS). The suction side (SS) is affected only by the impact of the smaller particles (up to 1 μm). Particular fluid dynamic phenomena, such as separation, stagnation point, and tip leakage vortex, strongly influence the impact location of the particles. [DOI: 10.1115/1.4028295]

Introduction

Gas turbines ingest a large amount of air during their operation. The quality and purity of the air entering the turbine is a significant factor in the performance and life of the gas turbine. In particular, the fouling of the axial compressor is a serious operating problem and its control is of critical importance for operators of gas turbine-driven power plants, compressor stations, and pump stations.

The air is a continuous medium that contains and carries a large number of particles (contaminants). The contaminants in the air are different in composition, size (pollen 50 μm, spores 3 μm–10 μm and exhaust particle < 0.1 μm), and quantity [1].

In order to minimize the performance loss of industrial gas turbines, an adequate filtration system that can limit the ingestion of contaminants by the power unit is required. For industrial gas turbines, highly effective filtration systems exist [2]. Because modern inlet filtration systems are effective in removing particles larger than about 1 μm to 2 μm (Fig. 1), compressor erosion is not a problem frequently found in industrial gas turbines. However, depending on the type of filtration system used, smaller particles can enter the engine. These smaller particles are too small to cause erosion issues, but they do cause compressor fouling. Evaluation of fouled compressors has revealed contamination both on the SS and the PS of the compressor blades [3]. Kurz and Brun [3] also pointed out that only small particles can stick to the blade surface and thus cause fouling. Morini et al. [4] and Aldi et al. [5] have shown by numerical simulation that the effects of fouling on the SS of blades are significantly stronger than from contamination on the PS.

The question that still requires research is the mechanism that allows particles to actually reach the suction surface. Particles that deviate from the streamlines will readily impact on the PS of the

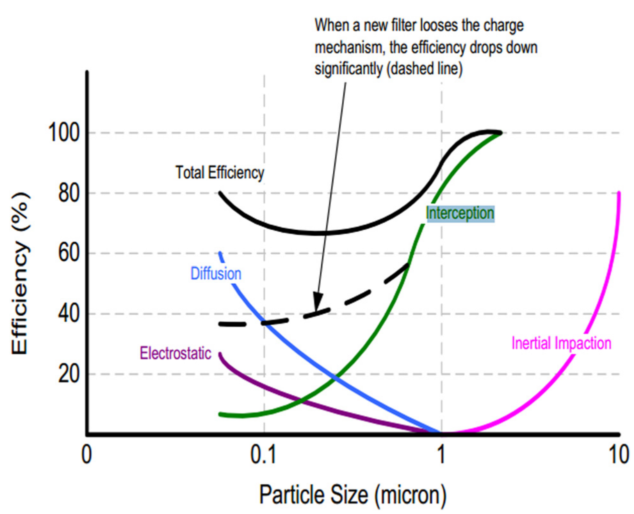

Fig. 1 Combination of filtration mechanism to obtain filter efficiency at various particle sizes [2]

Contributed by the International Gas Turbine Institute (IGTI) of ASME for publication in the Journal of Turbomachinery. Manuscript received July 21, 2014; final manuscript received August 4, 2014; published online xx xx, xxxx. Editor: Ronald Bunker.

blades, but the mechanism that can deposit particles on the SS of the blade is not fully understood.

In this article, an extended study on particles with diameters close to 1 μm was carried out. The results show the position and the quantity of the ingested particles that affected the blade surface of an axial compressor test case. Particular emphasis was placed on the modeling of the boundary layers, since the turbulent eddy structures are suspected to contribute to the impact of particles on the blade surface.

Literature Review

Compressor fouling is due to (i) the size, amount, and chemical nature of the aerosols in the inlet air flow, (ii) dust, (iii) organic matter such as seeds from trees, (iv) oil from leaky compressor bearing seals, and (v) ingestion of the exhaust or plumes from nearby cooling towers. Foulants in the ppm range can cause deposits on blading, resulting in severe performance deterioration. The effects of compressor fouling are a drop in airflow and compressor isentropic efficiency. Estimates have placed fouling as being responsible for 70–85% of all gas turbine performance losses accumulated during the operation. Output losses between 2% (under favorable conditions) and 15–20% (under adverse conditions) have been experienced [6]. Fouling can be removed by off-line water washing and slowed down by on-line water washing. However, water washing, as well as the loss of power, reduces the production capability of the gas turbine plant.

Particles that cause fouling are typically smaller than 2 μm. The conditions under which impacting particles actually stick to surface blades are less clear. In general, the sticking mechanisms include Van der Waals, capillary and electrostatic forces, and re-entrainment. The forces become more dominant for smaller particles. If there is wetness, capillary forces tend to dominate. This leads to the following conditions [3]:

- dry particles have to be very small to stick
- wet surfaces and/or wet particles allow bigger particles to stick.

The particle sticking on blade surfaces results in an increase of the thickness of the airfoil and the surface roughness. Both of these events change the flow path inside the passage vanes, in particular: (i) increment of the boundary layer thickness, (ii) decrement of the flow passage area, and (iii) modifications of the 3D fluid dynamic phenomena.

As mentioned above, the fouling was induced by particles smaller than 2 μm. From literature, the particle sizes can be categorized into seven classes [7]:

- Coarse solid: 5 mm–100 mm
- Granular solid: 0.3 mm–5 mm
- Coarse powder: 100 μm–300 μm
- Fine powder: 10 μm–100 μm
- Super fine powder: 1 μm–10 μm
- Ultrafine powder: $\sim$1 μm
- Nanoparticles: $\sim$1 nm

The fouling phenomena refer to the *ultrafine powder* category. In literature, there are many studies that have reported analyses of this type of particle. These studies are characterized by different models and dominated by different forces when the particle is transported and dragged by the air flow.

In this paper, three main issues are referred to: (i) CFD numerical simulations, (ii) particle treatment, and (iii) turbomachines. In this paragraph, the authors want to highlight the literature available regarding these three topics.

From a CFD point of view, some studies were related to understanding the capability of a commercial code to describe the trajectories of the particle that are dispersed and dragged by the stream airflow. Zhang and Chen [8] studied the particle distribution and the removal performance of the ventilation system in a ventilated room. The study was conducted for a particle size in the range of 0.31 μm–4.50 μm by using a Lagrangian method. The authors highlighted the model-method sensitivity to the number of trajectories and runs of the discrete phase simulations. In Ref. [9], the authors studied the influence of the model lift coefficients, the particle rotation and the influence of a two-way coupling resolution strategy. The results have shown that the formulation of the lift force and the rotation of the particle have an influence on the particle trajectories. Finally, the authors have shown that with the one-way coupling method the results were in strong agreement with the results obtained by a two-way coupling calculation.

From a particle point of view, in Ref. [10], the authors studied the influence of the impacting velocity and the nature of the particle on the erosion of different materials. The results have shown that the erosion was related to the presence of quartz in the dust and also that the threshold size limit (in order to avoid erosion) was equal to 5 μm (at about 305 m/s of impact velocity). From the experimental results, the authors have shown that the particle incurs a significant fragmentation which depends on the initial size and on the impact velocity.

From a turbomachinery point of view, in literature, there are studies related to the gas turbine and studies related to the axial compressor.

The first type was referred to the hot section of the gas turbine where high temperature plays a fundamental role in the particle transportation and sticking mode. Hamed et al. [11] reported a complete review of erosion and deposition research in turbomachines and the associated degradation in engine performance caused by particulate matter ingestion. In particular, the authors reported a large number of investigations on the particle deposition on the blade turbine surface, in which the characteristics of the particle motion, size and deposition rate of the particle were highlighted. The reported results show that in the particle size range of 0.5 μm–3.0 μm there is a combined action of two mechanisms called diffusion and inertia. On the turbine blade, in Ref. [12], there are specific experimental and numerical analyses in order to link the impact angle, impact velocity, and size particles to the erosion rate and surface roughness.

The second type, as mentioned above, was referred to the axial compressor. In Ref. [13], the authors performed a study of the erosion effects in an axial compressor stage. The particles have a diameter equal to 165 μm and the results were obtained with the following assumption: (i) nonrotating spherical particle, (ii) the particle–particle collision was neglected, (iii) the particle-phase had no influence on the gas-phase, and (iv) the drag force was the only force that influenced the particle-phase. The authors took into account the effect of the rebounded particles and the results show that the first impact of the particle determines the most important erosion on the blade surface, in particular, at the leading edge (LE). With the same axial compressor and nature of the particles, Suzuki and Yamamoto [14] show the performance drop and the modification of the flow path inside the stage caused by the erosion. Ghenaiet [15] studied the particle dynamics and erosion of the front compression stage of a turbofan PW-JT8-D17. Particle trajectory simulations used a stochastic Lagrangian tracking code and the sand particle size varied from 0 μm to 1000 μm. The numerical simulations show different trajectories for different particle diameters. After the initial impact, the larger particles were affected by inertia and centrifugal force and some of these re-impacted the blade surface at the PS. Some particles crossed the blade through the tip clearance and induced erosion of the blade tip. Small size particles (i.e., $\approx$10 μm) tended to follow the flow path closely and were strongly influenced by the flow turbulence, secondary flows, and flow leakage above the blade tip and induced erosion of the blade tip and shroud. Particles with a diameter less than 10 μm have not been taken into account for the erosion analyses.

In literature, regarding the fouling application and the ultrafine powder in axial compressors, there are some experimental results. Zuniga and Osvaldo [16], Parker and Lee [17], and Erol and

Bettner [18] have reported some experimental measurements with regard to the deposition on the axial compressor blade surface. In particular, in Ref. [16], there are reports that regard the deposits on the gas turbine compressor rotor and stator vanes for off/in-shore applications. In Ref. [17], there is a study of fouling patterns on blades caused by an ingestion of submicron particles (0.13 μm–0.19 μm). Finally, in Ref. [18], the authors report a comparison of the performance of gas turbine axial compressors for different shroud roughness levels.

While for the experimental evaluation of fouling, the data presented in literature cover some applications, from a CFD point of view, there is a lack of study. The fouling phenomena on the axial compressor can be well reproduced by a combined strategy that involves the modification of the thickness of the airfoil and the application of a surface roughness on the blade surface [19]. With this method, in Refs. [4] and [5], the authors presented some sensitivity analyses related to the different position of the deposits (pressure and SS, spanwise direction) on the blade surface by using the different values of surface roughness.

In this paper, the authors present a CFD study for the ultrafine powder ingestion (particle size 0.25 μm–2.00 μm) by an axial compressor rotor, the Nasa Rotor 37. The particle ingestion was studied by using a CFD commercial code. The main items of this work can be summarized as follows:

- validation of the numerical model by using the experimental data reported in literature
- simulation of the ingestion of an ultrafine powder
- quantitative analysis of the impact location
- sensitivity analyses of the particles–blade interaction in cases of different particle diameter.

Numerical Model and Validation

The geometry and performance data were taken from Ref. [20].

Reference Numerical Compressor Stage. The NASA Rotor 37 is composed of 36 blades and the tip clearance at design speed is 0.356 mm (0.45% of the blade span). Only a single passage vane was modeled as can been seen in Fig. 2(*a*).

All the simulations are performed in a steady multiple frame of reference in order to take into account the contemporary presence of moving and stationary domains. The rotating and stationary frames are coupled using a frozen stage interface with the appropriate frame transformation occurring across the interface. The numerical domain is composed by three domains: two stationary domains (inlet and outlet duct) and one rotating domain (rotor).

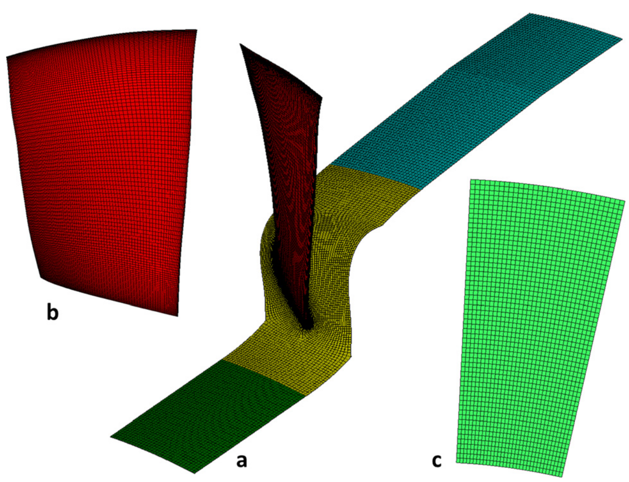

Fig. 2 NASA Rotor 37 numerical domain: (*a*) single passage vane, (*b*) the mesh on the blade surface, and (*c*) the mesh at the inlet surface

Numerical Grid. A multiblock hexahedral grid with a total number of 1,131,063 elements is used with refinements in the vicinity of the leading and trailing edges (TEs) of blade and near hub and shroud and in tip clearance. The mesh on the blade surface with the aforementioned refinements can be seen in Fig. 2(*b*). Regarding the near walls, the nodes are positioned in such a way that the values of y+ are within 5–65.

In Fig. 2(*c*), the detail of the mesh generated for the inlet surface can be seen. In this surface, every single element has the same size in order to guarantee a uniform node distribution on the surface. The uniform distribution of grid nodes allows the realization of a uniform particle injection from this surface. An inlet surface of 1,888 hexahedral elements was created.

Boundary Conditions. The total pressure, total temperature, and flow angle were imposed at the inflow boundary.

The inlet total pressure $p_{0,1}$ and total temperature $T_{0,1}$ were imposed at 101,325 Pa and 288.15 K, respectively. An average relative static pressure $p_{g,2}$ was imposed at the outflow boundary, both in the near-choked flow region and in the near-stall region. The outflow pressure was progressively increased in order to perform the entire performance trend.

All the simulations refer to 17,188 rpm (100% design rotational speed). Finally, since only a section of the full geometry has been modeled, rotational periodic boundary conditions were applied to the lateral surfaces of the flow domain.

Numerical Issues. The numerical simulations were carried out by means of the commercial CFD code ANSYS FLUENT 13.0 [21].

The code solves the 3D Reynolds-averaged form of the Navier–Stokes equations by using a finite-element based finite-volume method. An implicit Roe-flux-difference splitting (FDS) formulation was adopted with a Green-Gauss Node Based spatial discretization. For the flow, a second order Upwind was chosen.

Turbulence and Wall Modeling. In this paper, the standard k-ε turbulence model with a STandard Wall function (STW) is used. For the turbulent terms, a first order Upwind scheme was adopted for the solution phase.

Validation. In Fig. 3, the calculated and experimental performance maps [20] are reported. It can be noticed that the shape of both the experimental performance maps is correctly reproduced by the numerical code. Since the aim of the validation was to obtain a compressor model, the numerical model can be considered reliable. The numerical values are in fairly good agreement with the experimental data. The numerical pressure ratio β and the

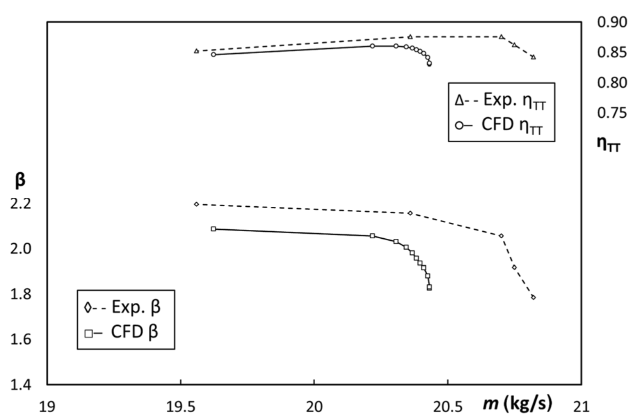

Fig. 3 Comparison between the experimental results (exp.) [20] and the CFD results

total-to-total efficiency η_{TT} always underestimate the experimental data but in a very consistent way. The deviation in terms of mass flow rate at the choked-flow condition is about 1.87%.

Particle Model

The fouling phenomena, as described above, are due to the adherence of materials and substances (liquid and/or solid) on the compressor surfaces, which alter both the shape and roughness of the surface progressively. This phenomenon can be described by the following three phases: (i) transport of the contaminants (discrete phase) by the air (continuum phase), (ii) contact and adhesion of the first discrete phase (particle) with the surface, and (iii) repeated adhesion of the following particles on the contaminant previously deposited on the surface.

The bond between two generic bodies (such as the first particle with the surface and the following particles with the particle that is already contact with the surface) is ruled by (i) the physico-chemical properties of the body, (ii) the type and characteristic of the impact (velocity and angle), and (iii) the presence of a third substance at the point of impact (called bridges). The phenomenon of the impact between two bodies, however, may not always result in an adhesion and bond between the two bodies. In fact, after impact, in some cases, the two bodies can change energy and directions of motion with respect to those possessed before the impact. In this case, the phenomenon can be described by the introduction of some parameters called coefficients of restitution.

A comprehensive study of the phenomenon of ingestion of contaminants by a turbomachine must contain the resolution of the three phases of adhesion and that of rebound mentioned above. In this paper, the transport of contaminants (particles) is resolved by the coupling of the Eulerian and Lagrangian approaches while, for the resolution of particles that impact the surfaces of the rotor, two strategies were adopted, i.e., the ideal adhesion and reflection.

Balance of Forces. CFD is a useful tool for studying particle dispersion, spatial distribution, and particle wall interaction with either the Eulerian or Lagrangian method. The Eulerian method treats particles as a continuum and solves the conservation equations for particle-phases. On the other hand, the Lagrangian method emphasizes the individual behavior of each particle and determines particle trajectories based on the equation of motion. In this paper, the solution approach is based on a mathematical model with Eulerian conservation equations in the continuous phase and a Lagrangian frame to simulate a discrete second phase. In this approach, the airflow field is first simulated, and then the trajectories of individual particles are tracked by integrating a force balance equation on the particle, which can be written as

$$\frac{du_p}{dt} = F_D + \frac{g(\rho_p - \rho)}{\rho_p} + F_S + F_B \qquad (1)$$

The left-hand side represents the inertial force per unit mass and u_p is the particle velocity. The first term on the right-hand side is the drag term (F_D is the inverse of relaxation time) and the second term represents the gravity and the buoyancy contribution, where ρ and ρ_p are the density of air and the particles, respectively. The last two terms F_S and F_B represent the additional contributions (per unit mass) called Saffman's lift and Brownian force, respectively. These last contributions are generally at least two magnitudes smaller than the drag force. However, some of these forces may occasionally become comparable in magnitude to the drag force within the turbulent boundary layer.

In this paper, the choice of the proper formulation of the drag terms represents the most important step because the particles that are ingested by the rotor add the following characteristics: (i) spherical, (ii) dragged by a high Mach number air flow, and (iii) its diameters are, in some cases, less than 1 μm. The software provides three types of drag model that are described below. The drag term for spherical smooth particles is

$$F_D = \frac{18\mu}{\rho_p d_p^2}\frac{C_D \mathrm{Re}_p}{24}(u - u_p) \qquad (2)$$

where μ is the fluid viscosity, d_p is the particle diameter, and Re_p is the particle Reynolds number defined as

$$\mathrm{Re}_p = \frac{\rho d_p |u_p - u|}{\mu} \qquad (3)$$

and C_D is the drag coefficient defined as

$$C_D = a_1 + \frac{a_2}{\mathrm{Re}} + \frac{a_3}{\mathrm{Re}^2} \qquad (4)$$

where a_1, a_2, and a_3 are the coefficients defined by Morsi and Alexander [22]. AQ3

If the particle Mach number is greater than 0.4 and the Reynolds particle number is greater than 20, for the proper resolution of the particle motion the spherical drag law must be corrected by the proper high Mach number term [23] provided by ANSYS FLUENT.

For the submicron size particles, the Stokes law was corrected by the Cunningham correction term. The drag term for spherical submicron particles follows the Stokes drag law

$$F_D = \frac{18\mu}{\rho_p d_p^2 C_c}(u - u_p) \qquad (5)$$

where μ is the fluid viscosity, d_p is the particle diameter, and C_c is the Cunningham correction factor defined as

$$C_c = 1 + \frac{2\lambda}{d_p}\left(1.257 + 0.4e^{-(1.1 d_p/2\lambda)}\right) \qquad (6)$$

where λ is the molecular mean free path.

The last two contributions are Saffman's lift force and Brownian force. Saffman's lift force is defined as

$$F_S = \frac{2K\nu^{1/2}\rho d_{ij}}{\rho_p d_p (d_{lk} d_{kl})^{1/4}}(u - u_p) \qquad (7)$$

where $K = 2.594$, d_{ij} is the deformation tensor, and ν is the air kinematic viscosity. This contribution is intended for small particle Reynolds numbers. Also Re_p based on the particle-fluid velocity difference must be smaller than the square root of the particle Reynolds number based on the shear stress Re_{sh} defined as

$$\mathrm{Re}_{sh} = \frac{d_p^2 |du/dy|}{\nu} \qquad (8)$$

The Brownian term is intended only for laminar simulations and its contribution has not been taken into account in this paper.

As mentioned above, every single model and contribution has its own application limit. For this reason, a preliminary sensitivity analysis has been carried out by the authors.

Tracking Method. The dispersion of particles in the fluid phase can be predicted using a stochastic tracking model. The time-averaged flow field determines the mean path of particles, while the instantaneous flow field governs each particle's turbulent dispersion from the mean trajectory. By computing the trajectory in this manner for a sufficient number of representative particles (named *number of tries*), the random effects of turbulence on the particle dispersion can be included.

This investigation used the discrete random walk (DRW) model to simulate the stochastic velocity fluctuations in the airflow. The DRW model assumes that the fluctuating velocities follow a Gaussian probability distribution. The DRW model may give non-physical results in strongly nonhomogeneous diffusion-dominated flows, where small particles should become uniformly distributed. Instead, the DRW will show a tendency for such particles to concentrate in low-turbulence regions of the flow. In this case, a specific analysis conducted by the authors shows that the interaction between the wall, with its boundary layer, and the discrete phase is characterized by the inertial law, as reported in more detail in the next paragraph. For this reason, the diffusion phenomena can be neglected and the DRW model can be considered reliable.

The number of particles tracked was selected in order to satisfy statistical independence since turbulent dispersion is modeled based on a stochastic process. In the present study, all the injections take place on the inlet surface (see Fig. 2(*c*)). The inlet surface was made by 1,888 uniform distributed elements that have the same size. This particularity allows the achievement of the maximum uniformity of the injected particles at the inlet of the rotor. All the injections were characterized by 1,500 trajectories and every single analysis was carried out with 3 different runs. For the tracking scheme the Runge–Kutta model was chosen.

Finally, according to Wang and Dhanasekaran [24], the time constant used in stochastic tracking was imposed equal to 0.15 for all the simulations.

Near-Wall Particle Behavior. As mentioned above, the particle–surface interaction and particle–particle interaction play a key role in the study of fouling. In literature, there are plenty of models that describe these two types of interactions. Tomas in Ref. [25] reported an extensive and comprehensive review of all the models present in the literature. Each model is necessarily obtained thanks to assumptions about the type of contact (elastic, elastic-adhesive, viscoelastic, plastic-adhesive) and the type of force–displacement (elastic–plastic, elastic-dissipative, plastic-dissipative, plastic-hardening, viscoplastic-adhesive). The particles adhesion (with a surface or another particle) can be explained by the following bond effects [25]: (i) surface and field forces at direct contact (Van der Waals forces, electrostatic forces, electric conductor, electric nonconductor, magnetic force), (ii) material bridges between particle surfaces (liquid bridges and solid bridges), and (iii) interlocking phenomena provided by macromolecular particle shape effects or by a particular particle nature or surface characteristics. These bond effects are directly related to forces and displacements that take place at a microscale level (close to the molecular size).

Finally, considering the dynamic movement and the subsequent contact of a particle with a surface (as may be the impact of a grain of dust and the rotor blade) the characteristics and phenomena that take place in the area of impact are directly related to the characteristics of the particle, the characteristics of the surface and the impact force, which can be represented by the impact velocity between the two bodies.

The goal of this paper is to provide an estimate of the presence of particles on the blade surfaces of the NASA Rotor 37 test case. As described above, the problem of the impact/adherence between two bodies is highly complicated and it is hard to be solved without using simplifications and assumptions. For this reason, the following conditions have been adopted: (i) not deformable spherical particles, (ii) ideal adherence condition (named *trap*) on the blade surface, and (iii) nonadherence condition (named *reflect*) on the hub and shroud surfaces.

In a generic way for the turbomachines applications, it can be possible to describe three types of resulting conditions for the contact between a particle and a surface: (i) a large particle bounces on a dry surface, (ii) a small particle sticks to a dry surface, and (iii) large and small particles stick to a wet surface. The condition of the ideal adherence set on the surface of the rotor blade reflects a real heavy operating condition, which is found in reality in cases where the compressor works in very humid environments and/or with the presence of oily substances which promote sticking (such as transmission oil and grease), as reported in Refs. [6] and [26].

The wall boundary conditions allow the evaluation of the position where the contaminants hit the blade surface for the first time, avoiding the introduction of the inaccuracies due to the use of restitution models not fully representative of the real conditions. The condition of nonadherence set on the hub and shroud allows the analysis only on the blade surfaces. The authors have implemented a specific functions and restitution coefficient for the near-wall particle behavior. The model functions are defined in agreement with the Ahlert model [27] where the impact angle function $f(\alpha)$ is defined as

$$f(\alpha) = 17.9\alpha - 33.4\alpha^2 \tag{9}$$

for the range 0–π/12. However, the function $f(\alpha)$ as defined as

$$f(\alpha) = 2.1843 + 1.0362\alpha + 0.5777\alpha^2 - 2.8201\alpha^3 + 1.4242\alpha^4 + 0.0618\alpha^5 - 0.1041\alpha \tag{10}$$

for the range $\pi/12$–$\pi/2$. The impact angle α is expressed in radians. The other model constants are: (i) the coefficient for the relative particle velocity $b(v)$ equal to 1.73 and (ii) the coefficient of the particle diameter $C(d_p)$ equal to 1.85×10^{-8}. The functions f, b, and C are related to the property of the materials.

For the restitution coefficient, the results obtained by Forder et al. [28] were chosen. In this study, the authors found the restitution coefficient for sand particles impacting steel plates. The restitution coefficient is dependent on the particle impingement angle α, and both the perpendicular and tangential components of the restitution coefficient should be considered. Forder et al. provided the following correlations for both perpendicular e_n, and tangential e_t, restitution coefficients based on impingement testing using AISI 4130 carbon steel and sand

$$e_n(\alpha) = 0.988 - 0.780\alpha + 0.190\alpha^2 - 0.024\alpha^3 + 0.027\alpha^4 \tag{11}$$

$$e_t(\alpha) = 1.000 - 0.780\alpha + 0.840\alpha^2 - 0.210\alpha^3 + 0.028\alpha^4 - 0.022\alpha^5 \tag{12}$$

where the impact angle α is expressed in radians.

The coefficients were implemented on the ANSYS FLUENT solver in order to describe the interaction between sand particles and blade surface well. Table 1 summarizes the location on the numerical model for all the functions shown.

For the particle–wall interaction, the turbulence model plays a key role in the resolution of the particle trajectory near the wall. Through the use of *k*-ε STW turbulence model, there is an isotropic treatment of the turbulence near the wall and this implies, in the case where the values of y+ are less than 5, that both the streamwise mean velocity and the turbulence kinetic energy will be overestimated. More details can be found in Ref. [29]. In this paper, as mentioned above, the values of y+ do not drop below 5.

Table 1 Wall–particle interaction settings

Location	DPM wall condition	Erosion model function $f(\alpha)$, $B(v)$, $C(d_p)$	Restitution coefficients e_n, e_t
Inlet duct	Reflect	✓	✓
Outlet duct	Reflect	✓	✓
Rotor (hub and shroud)	Reflect	✓	✓
Blade surface	Trap	✓	✗

Table 2 Characteristics of the injections

Case	1	2	3	4	5
Particle diameter, d_p (μm)	0.25	0.50	1.00	1.50	2.00
Stokes number, St	0.0010	0.0039	0.0158	0.0355	0.0630
Nondimensional relaxation time, τ^+	6	26	103	231	410
Filtration efficiency, η_f (%)	60	65	85	96	99
Total flow rate, m_p (kg/s)	3.51×10^{-6}	2.46×10^{-5}	8.43×10^{-5}	7.59×10^{-5}	4.50×10^{-5}

In Ref. [29], the authors report an extensive sensitivity analysis of the relationship between the turbulence models, mesh refinement close to the wall and particle dimensions expressed by the nondimensional particle relaxation time τ^+ defined as

$$\tau^+ = \frac{(\rho_p/\rho) d_p^2 u^2}{18\nu} \tag{13}$$

where the u is the flow shear velocity defined as

$$u = \sqrt{\frac{\tau_W}{\rho}} \tag{14}$$

and τ_w is the wall shear stress. Tian and Ahmadi [29] highlighted the effect of a different turbulence model on the velocity deposition for particles in a horizontal and vertical tube. Their study has shown that the k-ε STW turbulence model over-predicts the deposition velocity for particles in a *Brownian* ($\tau^+ < 10^{-2}$) and *transition* ($10^{-2} < \tau^+ < 10$) region and it does not allow the estimation of the real trend of the particle velocity deposition. For the *inertial* ($\tau^+ > 10$) region, the k-ε STW turbulence model over-predicts the deposition velocity but in a minor way compared to the other regions and the trend of the deposition velocity curve is in agreement with the other results. More details of the sensitivity analyses can be found in Ref. [29].

As can be seen in Table 2, the nondimensional particle relaxation time τ^+, defined by Eq. (13), is in the range of 6–410 which corresponds to the *inertial* region. For this reason the k-ε STW turbulence model used for all the analyses was considered suitable for studying the real deposition phenomenon that occurs in the axial compressor under investigation.

Injection. In order to take into account the real composition of the ultrafine powder, a density equal to 2,560 kg/m^3 was chosen. This assumption is due to the nature of the air contaminants that make up a large part of sand, pollen, and very small particles of soil. The variation of the particle diameter, d_p, is in the range of 0.25 μm–2.00 μm, while the Stokes number St (calculated at the inlet of the numerical model) is defined as

$$\mathrm{St} = \frac{\rho_p d_p^2}{18\mu} \frac{U_1}{d_h} \tag{15}$$

is in the range of 0.0010–0.0630.

All the analyses refer to injections having particles with the same diameter, the same material and therefore the same Stokes number. On the contrary, the total flow rate of the discrete phase m_p, is linked to the work environment of the compressor and the efficiency of the filtration system. In fact, as reported in Ref. [1], the particle concentration in the air χ depends on the working area of the turbomachine and there is also a connection between the filtration efficiency η_f and the particle diameter as reported in Ref. [2]. For this reason, the total flow rate of contaminants is defined as

$$m_p = \chi q M_p (1 - \eta_f) \tag{16}$$

where M_p represents the particle mass, the particle concentration χ refers to the city side working area with 100,000,000 particles/dm^3 and the filtration efficiency η_f refers to the good (but not optimal) charge conditions of the filter (see Fig. 1). All the simulation characteristics are reported in Table 2.

In order to achieve the uniform particle concentration assumption, particles were released at the same velocity as the freestream ($\approx$170 m/s). It is assumed that the particles will not affect the fluid flow (one-way coupling) as the volume fraction of the particles was very low ($\ll$10%). The continuum flow property refers to the noncontaminated flow conditions at the inlet of the compressor at the maximum efficiency point.

All injections take place on a previously solved flow field, at the best efficiency point. All results presented in this paper were obtained from convergent simulations, with a variation of the residues of the motion and turbulent equations close to zero.

Results

In this paragraph, the analyses of the particle impact on the NASA Rotor 37 are shown. Only a portion of particles injected from the inlet surface of the numerical model impacts on the blade surface, and due to the imposed surface condition (trap), the contact results in a permanent adherence. For the comparison among the studied cases, the ratio η_{hit} can be used. The η_{hit} is defined as the ratio between the number of particles that hit the blade and the total number of injected particles. The trend of the η_{hit} as a function of the particle diameter d_p is shown in Fig. 4.

From Fig. 4, it is possible to observe that the percentage of the particles that hit the blade surface increases with the diameter of the particles (solid line), with a law very similar to the variation of the Stokes number (dashed line). The same result, not shown for brevity, is obtained by comparing these two trends with the trend of the nondimensional particle relaxation time τ^+, defined in Eq. (13). The increase of impacting particles with increasing nondimensional relaxation time is consistent with the indications given in Ref. [29]. In Fig. 4, the total number of particles injected and the absolute number of impacting particles on the blade surface are also reported.

Due to the wall–particle interaction settings, the particles do not stick to the hub and shroud. Particles bounce on these surfaces following the rules imposed by the restitution coefficients reported in Eqs. (11) and (12). In Table 3, the global count of the bounces is reported. The values of N_b represent the number of particles that bounce on the hub or shroud, the values of n_b represent the ratio between the number of particles that bounce on the hub or shroud and the total number of injected particles and finally, the values of b represent the average number of bounces of each particle.

It can be noticed that the number of bouncy particles increases with the increase of particle diameter but, conversely, the number of average bounces decreases with the increase of particle diameter. This implies that for the smaller diameters, the particles that hit the blade may have had more frequent multiple impacts on the hub or shroud before the impact with the blade. Thus, the smaller particles could have a better chance of sticking to the hub or shroud surface compared to the bigger ones. However, this phenomenon is related to a much smaller number of particles

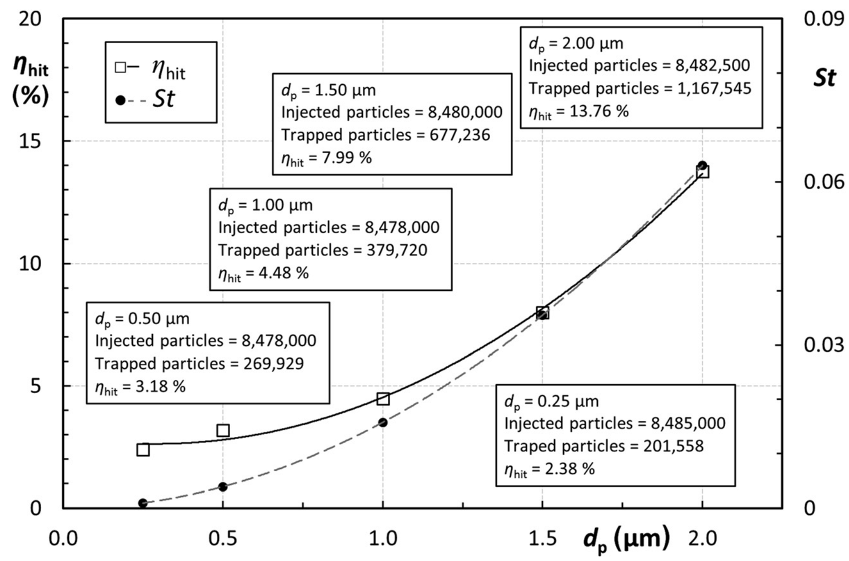

Fig. 4 Capture efficiency η_{hit} and Stokes number St versus particle diameter d_p

Table 3 Particles bounces on the hub and shroud

	Hub			Shroud		
d_p (μm)	N_b	n_b (%)	b	N_b	n_b (%)	b
0.25	66,186	0.78	4.4	66,216	0.78	6.8
0.50	71,154	0.84	2.5	76,236	0.90	6.7
1.00	53,082	0.63	1.3	94,218	1.11	6.4
1.50	63,357	0.75	1.1	122,811	1.45	5.4
2.00	91,749	1.08	0.9	160,617	1.89	4.2

compared to the number of injected particles (less than 2.00%) and does not influence the overall results.

Particle Concentrations. The first analysis of the results refers to the quantity defined as discrete phase model (DPM) concentration χ_{DPM}, which allows the concentration of contaminant on a specific surface, defined as kg/m^3, to be determined. The χ_{DPM} allows the combined effects between the trajectories of the particles and the total mass flow rate m_p calculated according to Eq. (16) to be highlighted. In the present paper, the χ_{DPM} allows the evaluation of the combined effects of: (i) the particle trajectories, (ii) the contamination intensity of the working compressor place χ, and (iii) the filtration efficiency η_f. The selected surface to evaluate the χ_{DPM} was obtained by a transformation of the blade surface. In particular, the new surface was positioned at a constant distance from the blade surface of 50 μm for each point. In this way, it is possible to evaluate the presence of contaminants in the portion of fluid that is located very close to the blade surface. Figure 5 shows the contour plot of χ_{DPM} on the transform surface for PS and SS of the blade. From this contour plot, it is possible to notice that

- the peak of the contaminants concentration is found in correspondence to the LE;
- the PS is more contaminated than the SS;
- the injections with the smallest particle ($d_p = 0.25$ μm and $d_p = 0.50$ μm) show a more distributed contaminant concentration on the PS, even if for the particles with d_p equal to 0.50 μm it is possible to see a band without contaminants at about 40% of the span;
- the injections with the largest particle ($d_p = 1.50$ μm and $d_p = 2.00$ μm) show a relevant concentration of contaminants only on the PS, while in the SS, it is possible to see a very small quantity of contaminants close to the hub and the top of the blade.

A detailed analysis of the particle impact zones on the blade surface will be carried out in the following paragraphs. The DPM concentration shown in Fig. 5 refers to one of the three runs. In fact, as mentioned above, every case was repeated for three different runs in order to avoid the problems caused by statistical resolution of particle tracking. In Table 4, the values of the DPM concentration peak χ^*_{DPM}, and the values obtained by a weight-area average of the DPM concentration $\tilde{\chi}_{DPM}$ for all of the executed runs are reported. Due to this evidence, it is possible to define an average value $\overline{\chi}_{DPM}$ of the $\tilde{\chi}_{DPM}$ among the three runs for each case. From the values of Table 4, it is possible to note that the values obtained for the three runs of each case are very close to each other, confirming the independence of the results from the statistical dispersion. The values reported in Table 4 are higher compared to the values characteristic of actual air contaminant concentration (<500 μg/m^3). This fact is due to the previous assumption of particle size, distribution and matter density: actual air contaminants are a distribution of particles of different sizes and materials as reported in Ref. [1] and not particles with a homogenous size and density as assumed in the numerical simulations.

Figure 6 shows the trend of the m_p and $\overline{\chi}_{DPM}$ as functions of the particle diameter d_p. It is possible to note that for Case 3, corresponding to particles with a diameter equal to 1.00 μm, the operating condition for the compressor is the most affected by the contaminants. In fact, for this case the highest values of m_p are associated with the highest values of $\overline{\chi}_{DPM}$.

From the $\overline{\chi}_{DPM}$, the ratio H can be defined as

$$H = \frac{\overline{\chi}_{DPM}}{\chi M_p (1 - \eta_f)} \tag{17}$$

This represents the dimensionless index of the compressor's capacity to concentrate the contaminants in the vicinity of the blades. For the studied cases, this particular index assumes the values reported in Table 4. This ratio is a representative index of a real fouling condition in which the compressor operates.

In fact, from this index, it is possible to link the characteristics of (i) the amount of contaminants, (ii) the type of contaminants, (iii) the filtration efficiency, and (iv) the flow pattern inside the axial compressor. The most severe fouling condition that affected the Rotor 37 at the best efficiency point is Case 3 for which all the

ID: sethuraman.m Time: 12:35 I Path: W:/3b2/TURB/Vol00000/140051/APPFile/AS-TURB140051

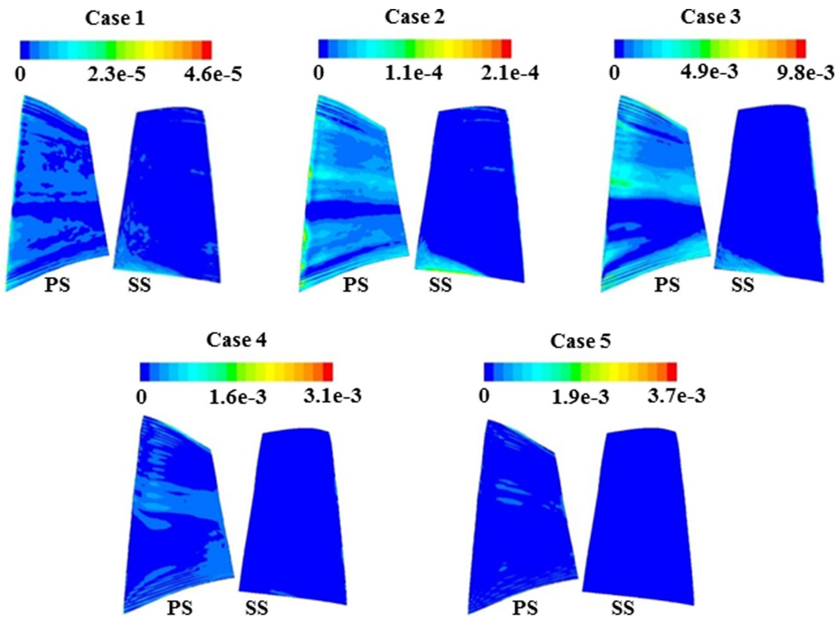

Fig. 5 DPM concentrations (kg/m^3), PS and SS

Table 4 DPM concentrations (μg/m^3) and fouling index

	1st run		2nd run		3rd run		Average	
d_p (μm)	χ^*_{DPM}	$\tilde{\chi}_{DPM}$	χ^*_{DPM}	$\tilde{\chi}_{DPM}$	χ^*_{DPM}	$\tilde{\chi}_{DPM}$	$\bar{\chi}_{DPM}$	H
0.25	4.6×10^4	1.9×10^3	4.6×10^4	1.9×10^3	4.5×10^4	2.0×10^3	1.9×10^3	0.29
0.50	2.2×10^5	1.5×10^4	2.2×10^5	1.4×10^4	2.1×10^5	1.4×10^4	1.4×10^4	0.31
1.00	9.8×10^6	5.0×10^5	1.0×10^7	5.0×10^5	9.6×10^6	4.9×10^5	5.0×10^5	3.09
1.50	3.1×10^6	7.4×10^4	3.0×10^6	7.5×10^4	3.1×10^6	7.4×10^4	7.4×10^4	0.51
2.00	3.7×10^6	5.3×10^4	3.6×10^6	5.3×10^4	3.7×10^6	5.3×10^4	5.3×10^4	0.61

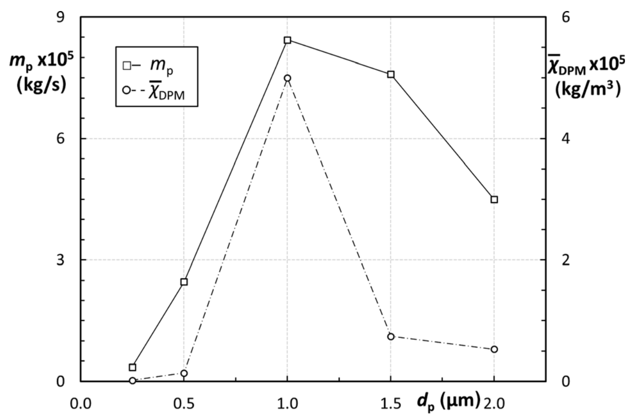

Fig. 6 Average DPM concentration and total mass flow m_p versus particle diameter d_p

four (i–iv) aforementioned characteristics determine the highest value of the index.

The index H is very similar to the mass transfer coefficient h_f found in Parker and Lee [17], which defines the ratio of the mass deposited per unit area per unit time and the mass concentration in air per unit volume. While the mass concentration in air per unit volume is the denominator in Eq. (17), the numerator of the h_f can be obtained by the quantity called *Accretion Rate* provided by the software. The authors have instead used the ratio H, that appears to be independent of time for two reasons: (i) the trap conditions on the blade surface implies unrealistic values of the quantity *Accretion Rate*, in contrast to those obtained from experimental tests reported by Parker and Lee and (ii) the ratio H defined in Eq. (17) can be used to compare different types of machine considering only the capacity of the compressor to concentrate the air contaminants around the blade surface (due to the shape of the hub, shroud, airfoil).

Particle Impact Locations. In this paper (the first of two), the authors have highlighted the locations affected by the particle impact. Theoretically, zones with a high number of impacts will be more affected by the fouling phenomena, but, actually, the fouling phenomena depend on the sticking characteristic of the particles. A comprehensive analysis on the sticking characteristics and real fouling phenomena on the blade surface are reported in the second paper [30].

In this paragraph, the analysis of the results refers to the impact location of the particles on the blade surface. It can be noticed that

- by increasing particle diameter d_p, the SS is less affected by the impacts. There are a greater number of impacts on the PS. In Fig. 7, the trends of the impacting particles on the blade (for both sides) for all the cases can be seen. The η_{hit} values reported for the PS $\eta_{hit,PS}$ and SS $\eta_{hit,SS}$ refer to the percentage of particles that hit the PS or SS compared to the total number of injected particles. As can be seen from Fig. 7, the particles tend to hit the PS in increasing quantities as the particle diameter increases. These distributions are very important from operators' points of view, because the capability of the compressor to collect air contaminant is directly related to the power unit performance drop. In Fig. 7, the η_{side} values are reported in pie charts. These values refer to the

ID: sethuraman.m Time: 12:35 I Path: W:/3b2/TURB/Vol00000/140051/APPFile/AS-TURB140051

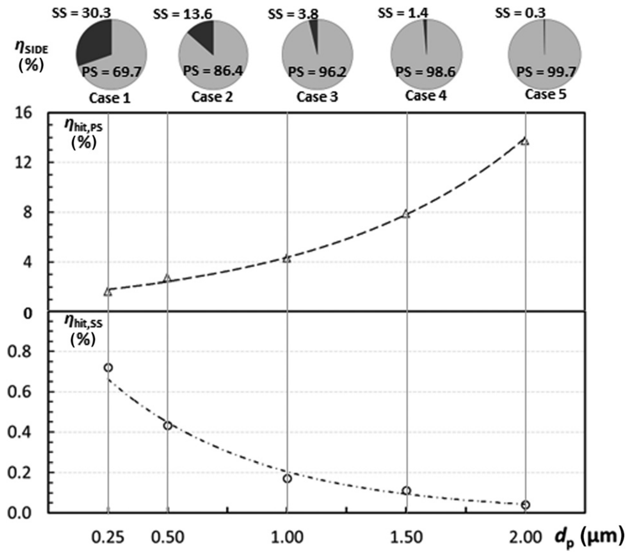

Fig. 7 Particle impact distributions, PS and SS

percentage of particles that hit the blade on PS or SS compared to the total number of particles that hit the blade. This result is in line with those reported in literature regarding (i) fouling characterized by particles with dimensions close to the unit of micron [3] and (ii) erosion of rotor blades which is characterized by larger particles [15]. In fact, the fouling phenomenon is characterized by a wider distribution of the particle on the blade surfaces with respect to erosion that shows a higher percentage of impacts on the PS than on the SS;

- for cases 1 and 2, in which the particles have a diameter equal to 0.25 μm and 0.50 μm, respectively, particles impact on the entire height of the blade in the SS; in all cases, particles impact 25% (up to 3rd strip) of the blade height in the SS. In particular, the presence of particles that hit the rear part of the airfoil can be seen in cases 3, 4, and 5. This phenomenon is due to the separation and consequent three-dimensional vortex that drags the contaminants into the vicinity of the hub, as can be seen in Fig. 8, which highlights the low particle velocity zone close to the hub. Analogous results can be found in Ref. [31] where field data regarding the deposition of foulants on a transonic blade compressor are reported. Silingardi et al. [31] reported the blade surface condition after 25,000 operation hours and the authors highlighted that three-dimensional flow features cause small particles to be deposited in zones where secondary flows and vortices are dominant;
- in correspondence to the blade tip, the presence of impacts on both sides of the blade can be noticed. For the largest particles (1.50 μm and 2.00 μm), the presence of impacting particles on the SS dragged into that area by the tip leakage vortex can be noticed. In fact, the presence of the tip gap (equal to 0.356 mm) causes the tip leakage vortex that drags the particles from the PS to the SS of the blade, as can be seen in Fig. 8;
- there are particular impact patterns in the first portions of the chord, where there is a high presence of impacting particles on the LE and, by contrast, there are no particles in the area immediately downstream. This effect, highlighted in Fig. 9, is due to the phenomena of stagnation induced from the nose of the airfoil. In Fig. 9, it is possible to observe the pattern of impact (Case 1), for the 6th strip (47% of span) and the contour plot of the air velocity of a blade-to-blade surface superimposed. In Fig. 9, for both the SS and PS, the phenomenon of stagnation that influences particle impact on the blade surface can be seen.

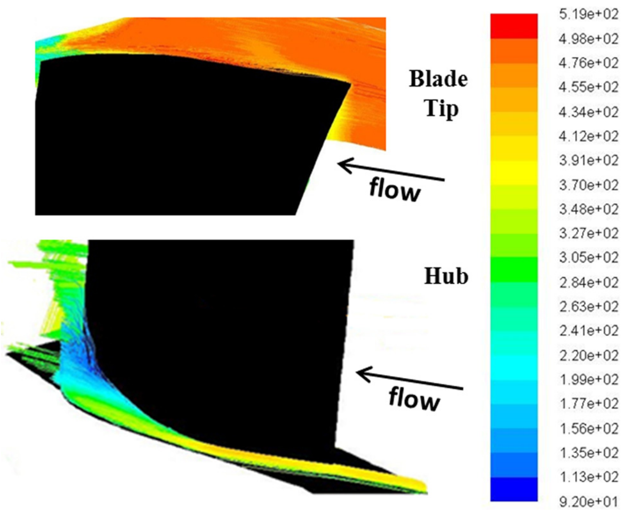

Fig. 8 Particle trajectories (colored by velocity (m/s)) at the hub and at the blade tip, SS, case 2

In the Appendix, an overall representation of the impact zone is reported.

In order to show the obtained results in a general form, useful for comparative analysis, some new quantities are introduced in this paper. The new quantities refer to the impact concentration on the blade surface.

The first quantity is defined as the percentage of impact concentration on the strip

$$X_{\mathrm{STRIP}} = \left[\frac{\text{No. impacts at strip}}{\text{No. impacts at blade}}100\right]\frac{1}{A_{\mathrm{STRIP}}} \qquad (18)$$

where A_{STRIP} refers to the strip area. By using X_{STRIP} values, it is possible to highlight the impacts along the spanwise direction of the blade.

As can be seen from Fig. 10, all cases show the smallest number of impacts for the 5th strip. The impact distribution assumes the same qualitative trend for all cases: (i) a high percentage of impacts in correspondence to the strips closest to the hub (1st and 2nd strip, 3% and 12% of the span, respectively) probably due to the shape of the hub and to the fluid dynamic phenomena that are mentioned above and highlighted in Fig. 8, (ii) a small percentage of impacts in the middle of the blade height (5th and 6th strip, 38% and 47% of the span, respectively), and (iii) a high percentage of impacts in correspondence to about 60% of the span.

The presence of impacting particles at the blade tip (11th strip) grows with the increase of the particle diameter and plays a key role directly related to compressor performance. As reported by Aldi et al. [5], the effects of fouling at the blade tip (e.g., the increase in surface roughness) have a greater influence on the compressor performance degradation.

From the analysis of the chart reported in Fig. 10, it can be notice that the impacts on the 10th and 11th, 83% and 94% of the span, respectively, are comparable with the impacts that occur on the rest of the blade. This result highlights how all the particle diameters are potentially suitable for generating a real compressor performance drop.

The distribution of the particle impact along the blade span is slightly influenced by the wall–particle interaction settings. In fact, only a small percentage of the particles that hit the blade bounce from the shroud or from the hub to the blade surface. In particular, for Case 3 ($d_p = 1.00\,\mu$m) this percentage reaches the maximum value, 5%, while for the other cases, this percentage is about 3%. Thus, the nonadherence condition (*reflect*) imposed on the hub and shroud surfaces does not limit the generality of the results.

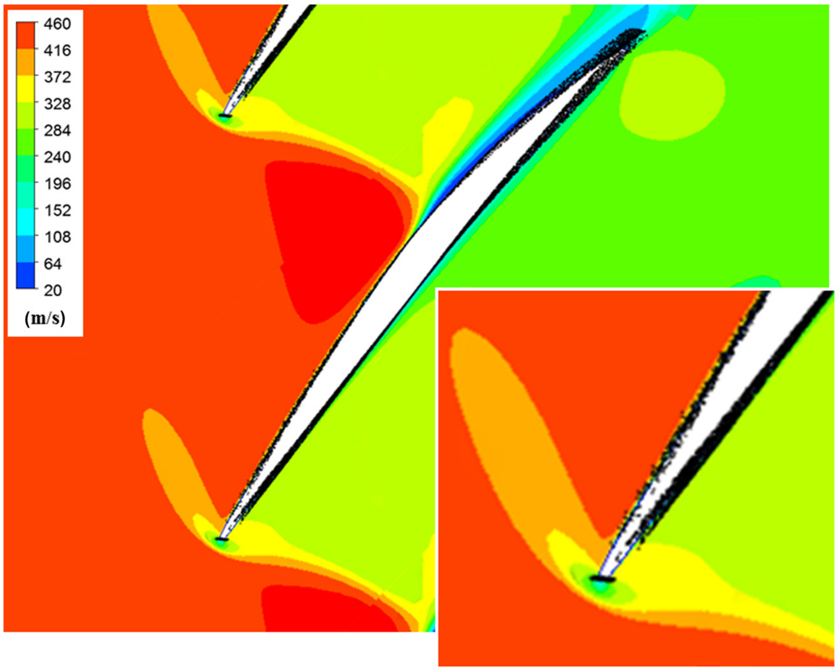

Fig. 9 Blade-to-blade velocity contours and impact patterns superimposed, 6th strip, case 1

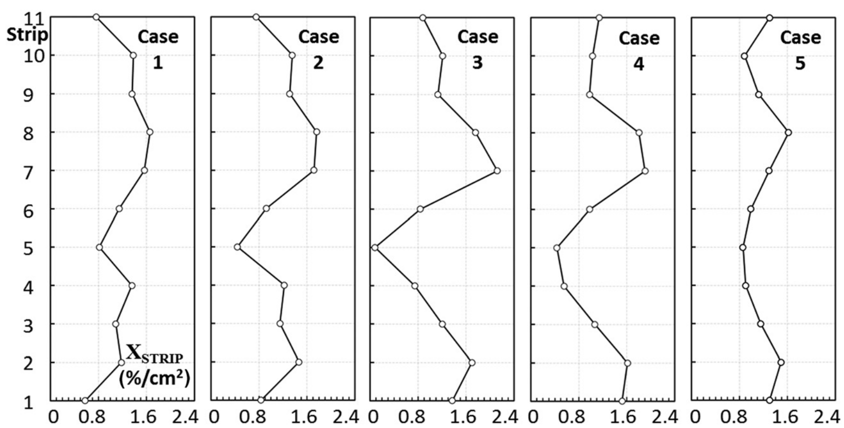

Fig. 10 Impact strip concentrations X_{STRIP}

From a fouling point of view, the most interesting results refer to Case 1, with particle diameter equal to 0.25 μm. In fact, even if the number of particles that hit the blade surface is the smallest (see Fig. 4) the particles are present both in PS and SS.

A more significant and detailed analysis of the impact locations on the blade surface for Case 1 ($d_p = 0.25\ \mu$m) can be observed in Fig. 11. In this graph, concerning the 2nd, 6th, and 10th strips (12%, 47%, and 83% of the span, respectively) the impact patterns along the chord for a specific strip can be noted.

The quantity reported in Fig. 11 is defined in agreement with the other one defined in Eq. (18).

In this case, the impact concentrations X_{SLICE} refer to the amount of impacts in a single slice obtained by a chordwise division of the strip with respect to the total number of particles that impact the entire considered strip

$$X_{SLICE} = \left[\frac{\text{No. impacts at slice}}{\text{No. impacts at strip}} 100\right] \frac{1}{A_{SLICE}} \tag{19}$$

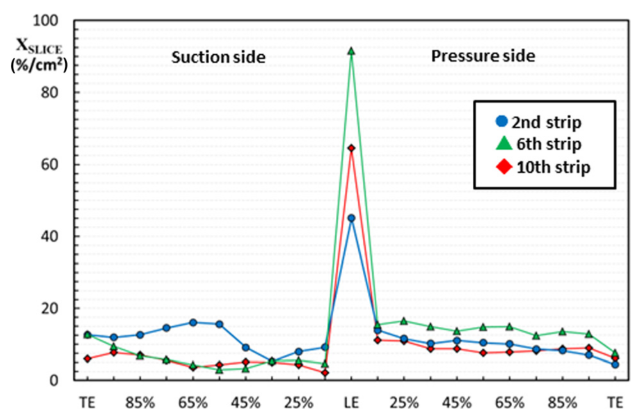

Fig. 11 Particle distributions X_{SLICE}, 2nd, 6th, and 10th strip, case 1

Table 5 Impact concentrations, case 1

Strip	$A_{\mathrm{STRIP,SS}}$ (cm^2)	$X_{\mathrm{STRIP,SS}}$ (%/cm^2)	$X_{\mathrm{hit,STRIP,SS}}$ (%/cm^2)
1	2.72	1.262	0.018
2	4.11	2.458	0.034
3	3.94	2.138	0.030
4	3.63	2.595	0.036
5	3.62	1.789	0.025
6	3.61	2.027	0.028
7	3.58	2.945	0.041
8	3.59	3.657	0.051
9	3.61	2.683	0.037
10	5.09	2.685	0.037
11	5.58	1.391	0.019

where A_{SLICE} refers to the area of the slice obtained by a chordwise division of the strip. The adopted chordwise division is reported in abscissa for each distribution. Figure 11 shows the impact distributions in terms of X_{SLICE} for the 2nd, 6th, and 10th strips. From Fig. 11, the high percentage of impacts on the LE can be noted which, in relative terms to the impacts on the strip, reaches a peak for the 6th strip (i.e., at midspan). A similar phenomenon can also be found in the experimental measurements reported by Parker and Lee [17] where the authors provided some deposition tests for a turbine blade.

The strip closest to the hub (2nd strip) shows a more uniform impact distribution on the blade surface, affecting the SS more than the PS. In the strip at the top of the blade (10th strip), there is a high impact concentration on LE and a low impact concentration on TE if compared to the other two strips. For all the shown impact distribution trends on the strips, a different decreasing trend of the number of impacts between PS and SS can be noticed. In fact, in the PS at the portion of the chord immediately after the LE, there are a number of impacts comparable what occurs in the remaining slices. On the contrary, in the SS, there is a nonuniform decreasing trend of the number of impacts. In fact, there are a smaller number of impacts in the slice immediately next to the LE with respect to slices corresponding to higher chords. In particular, the peak of impacts for the TE in the 2nd and 6th strip are highlighted. The analysis of impacts on the SS plays an important role, such as the one conducted at the tip of the blade because it is directly related to the loss of performance for fouled compressors. As pointed out by Morini et al. in Ref. [4], the effects of fouling on the SS (e.g., the increase in surface roughness) have a greater influence on the compressor performance degradation. For this reason, in the next paragraph, the authors present a dedicated analysis regarding particle impacts on the SS obtained from the results of Case 1 ($d_p = 0.25\ \mu$m).

SS Analyses. The first analysis on particle impacts for the SS is conducted by introducing a quantity in agreement with the other defined in Eq. (18). In this case, the impact concentration $X_{\mathrm{STRIP,SS}}$ refers to the number of impacts in a single SS strips compared to the total number of impacts affecting the entire SS

$$X_{\mathrm{STRIP,SS}} = \left[\frac{\text{No. impacts at strip, SS}}{\text{No. impacts at SS}} 100\right] \frac{1}{A_{\mathrm{STRIP}}} \qquad (20)$$

Table 5 reports the different values of $X_{\mathrm{STRIP,SS}}$ for each strip. Unlike the trends reported in Fig. 10, the values are very similar. In this case, there is not a clear decrease in the number of impacts in correspondence to the 5th strip. The SS is affected by a fairly large number of impacts in the highest strips (8th–11th) for which the fouling sensitivity is the highest [4,5].

In Table 5, the values of the $X_{\mathrm{hit,STRIP,SS}}$ are also reported. The $X_{\mathrm{hit,STRIP,SS}}$ is defined by the ratio of the amount of impacts in a single SS strip compared to the total number of injected particles. These values have the same importance for the gas turbine operators as the values reported in Fig. 7.

In Fig. 12, the impacts distributions on the entire SS can be seen. The quantity used to represent the results is the same as the one used in Fig. 11 and defined by Eq. (19). To improve the reading of the contour, the values of LE and TE were omitted.

The greatest SS impact concentration takes place in the front (close to LE) and in the rear (close to TE). In fact, the peaks of the impact concentration are carried out at the end of the profiles at the 2nd and 8th strip. Only a small portion of the SS, in correspondence to the 6th strip and approximately at half chord, is almost completely free from impacts. The impact pattern of the SS shows a peculiarity due to a specific fluid dynamic phenomenon. As reported by Parker and Lee [17], the collision of the particles takes place in the areas preceding and following the area (line) of flow separation from the blade. As shown in Fig. 12, the overlapping (qualitative because of the projection on the plane) of the impact contour and the separation line (obtained by the shear stress contour plot) shows the correspondence of the two effects. This phenomenon is also evident from Fig. 12, in which the number of impacts in the SS has a much less uniform trend than those related to the PS, where the flow separation does not take place. From Fig. 12, the chordwise coordinates at which the flow separation from the blade surface occurs can be distinctly identified. In particular: (i) for the 2nd strip the separation occurs at 30–35% of

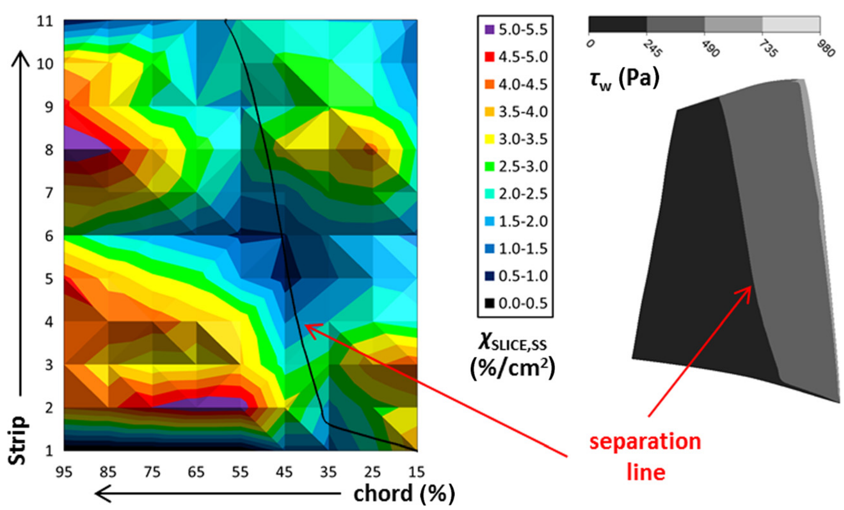

Fig. 12 Shear stress and deposition contour plots $X_{\mathrm{SLICE,SS}}$ with the separation line superimposed, case 1

the chord, (ii) for the 6th strip the separation occurs at 50% of the chord, and finally (iii) for the 10th strip the separation occurs for 65% of the chord.

Conclusions

In this paper, an extended study on microparticle ingestion by an axial stage compressor was carried out. Modern air filtration systems for industrial gas turbines will only remove a portion of these particles from the airstream. These small particles are responsible for compressor fouling if they come into contact with the compressor airfoils and stick there. For this reason, by using a Eulerian–Lagrangian numerical CFD approach, the authors have studied the interaction of ultrafine powder with the blade surface.

The numerical model and the particle model have been validated by the experimental and numerical data reported in literature. Special attention was given to the particle–wall interaction in terms of turbulence model wall treatment and in terms of the restitution coefficients. Using realistic air contamination data, the filtration efficiency of state of the art air filtration systems, and the size of the axial compressor, we obtained results for both the particle trajectories (including the impact zones on the blade surface), and the magnitude of fouling which can afflict the axial compressor.

The key results can be summarized as follows:

- the percentage of particles that hit the blade surface increases with the diameter of the particles with a law very similar to the variation of the Stokes number;
- the most severe fouling conditions that affected the Rotor 37 at the best efficiency point, is for particles with a diameter equal to 1.00 μm;
- with the increasing particle diameter the SS is less affected by the impacts that take place in a greater quantity on the PS;
- particular fluid dynamic phenomena such as tip vortex due to the tip leakage, separations, and stagnation point determine and influence the impact patterns;
- the analysis of the impact locations obtained for the smallest particles showed different trends for the PS and the SS due to the different fluid dynamic phenomena.

The understanding of fouling mechanisms in compressors is still a challenge for manufacturers and users. An increase in the knowledge of fouling through the use of numerical codes may therefore constitute a decisive element for better planning of maintenance of turbomachinery. In this sense, the second part of this work will focus on impact kinematics analysis and particle sticking phenomena in order to better describe and understand particle–blade interaction.

Nomenclature

A = area
a_1,a_2,a_3 = model coefficient
b = bounce (average)
B = function (referred to erosion model)
C = function
d = diameter
d_{ij} = deformation tensor
e = restitution coefficient
f = function (referred to impact angle)
F = force
g = gravity acceleration
H = fouling index
h_f = mass transfer coefficient
k = turbulent kinetic energy
K = model constant
m = mass flow rate
M = mass
N = total particles (referred to particles)
p = pressure
q = volume flow rate
Re = Reynolds number
St = Stokes number
t = time
T = temperature
u = velocity
U = averaged velocity
v = relative velocity particle
X = impact concentration (blade)
y^+ = nondimensional distance

Greek Symbols

α = impact angle
β = compression ratio
ε = dissipation rate of turbulent kinetic energy
η = efficiency
λ = molecular mean free path
μ = dynamic viscosity
ν = kinematic viscosity
ρ = density
τ = shear stress
τ^+ = nondimensional particle relaxation time
χ = particle concentration (air)

Subscripts and Superscripts

b = bounce
B = Brownian
c = Cunningham
D = drag
f = filtration system
g = gauge
h = hydraulic
hit = hit (referred to particle–blade interaction)
l,k = indices
n = normal direction
p = particle
S = Saffman
sh = shear
SIDE = side (referred to the side of the blade)
SLICE = slice (referred to chordwise division)
STRIP = strip (referred to spanwise division)
t = tangential
TT = total-to-total
w = wall
0 = total
1 = inlet
2 = outlet
— = average
∼ = weighted-area average
* = peak

Acronyms

DPM = discrete phase model
DRW = discrete random walk
CFD = computational fluid dynamics
FDS = flux-difference splitting
LE = leading edge
PS = pressure side
SS = suction side
STW = STandard Wall function
TE = trailing edge

Appendix: Overall Impact Patterns

All the particle impact patterns in Fig. 13 are reported. Each pattern represents the projection of the fouled airfoil into a perpendicular plane with respect to the spanwise direction. On the left side, the spanwise station and the correspondent percentage of

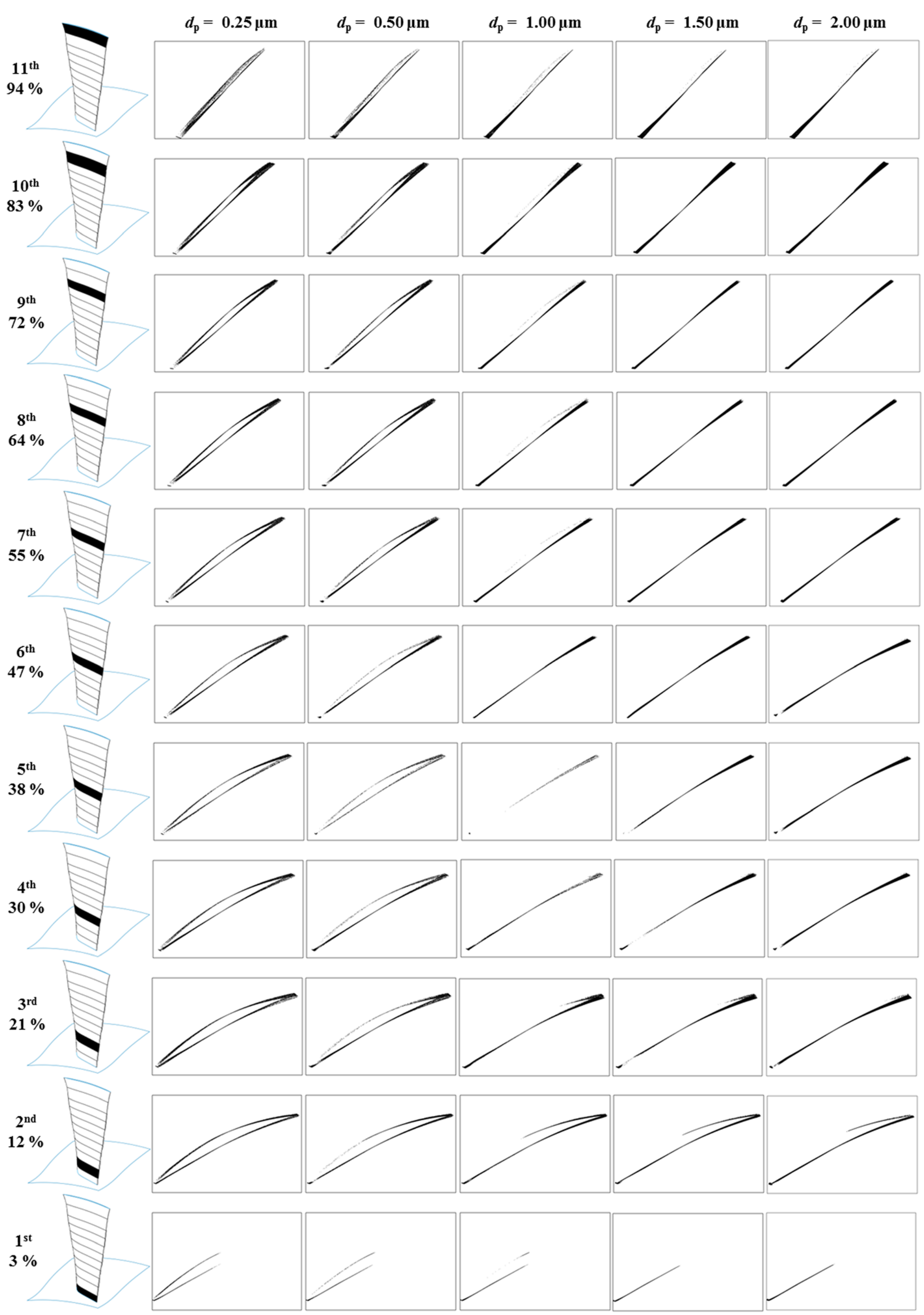

AQ4

Fig. 13 Spanwise subdivision (left side) and overall impact patterns

the blade span can be seen. The blade was divided by 11 strips along the spanwise direction and each dot on the graph represents a single particle that has hit the blade surface. Due to the shape of the hub, which develops along the streamwise direction with different diameters, the projection of the first strip is not complete and only the first half of the airfoil can be represented.

References

[1] camfil FARR, 2013, Technical Report No. ■. AQ5
[2] Wilcox, M., Kurz, R., and Brun, K., 2012, "Successful Selection and Operation of Gas Turbine Inlet Filtration Systems," Proceedings of the 14th Turbomachinery Symposium, Houston, TX. AQ6
[3] Kurz, R., and Brun, K., 2012, "Fouling Mechanism in Axial Compressors," ASME J. Eng. Gas Turbines Power, **134**(3), p. 032401.

[4] Morini, M., Pinelli, M., Spina, P. R., and Venturini, M., 2011, "Numerical Analysis of the Effects of Non-Uniform Surface Roughness on Compressor Stage Performance," ASME J. Eng. Gas Turbines Power, **133**(7), p. 072402.

[5] Aldi, N., Morini, M., Pinelli, M., Spina, P. R., Suman, A., and Venturini, M., 2014, "Performance Evaluation of Non-Uniformly Fouled Axial Compressor Stages by Means of Computational Fluid Dynamics Analyses," ASME J. Turbomach., **136**(2), p. 021016.

[6] Kurz, R., Brun, K., Meher-Homji, C., and Moore, J., 2012, "Gas Turbine Performance and Maintenance," Proceedings of the 41st Turbomachinery Symposium, Houston, TX.

AQ7 [7] FLUENT, Software Training.

[8] Zhang, Z., and Chen, Q., 2006, "Experimental Measurements and Numerical Simulations of Particle Transport and Distribution in Ventilated Rooms," Atmos. Environ., **40**(18), pp. 3396–3408.

AQ9 [9] Gupta, P. K., and Pagalthivarthi, K. V., 2006, "A Comparative Study of Effect of Model Lift Coefficients on Particle Trajectory," Ind. J. Eng. Mater. Sci., **13**(■), pp. 293–306

[10] Goodwin, J. E., Sage, W., and Tilly, G. P., 1969, "Study of Erosion by Solid Particles," Proc. Inst. Mech. Eng., **184**(15), pp. 279–292.

[11] Hamed, A., Tabakoff, W., and Wenglarz, R., 2006, "Erosion and Deposition in Turbomachinery," J. Propul. Power, **22**(2), pp. 350–360.

[12] Hamed, A. A., Tabakoff, W., Rivir, R. B., Das, K., and Arora, P., 2005, "Turbine Blade Surface Deterioration by Erosion," ASME J. Turbomach., **127**(3), pp. 445–452.

[13] Suzuki, M., Inaba, K., and Yamamoto, M., 2008, "Numerical Simulation of Sand Erosion Phenomena in Rotor/Stator Interaction of Compressor," J. Thermal Sci., **17**(2), pp. 125–133.

[14] Suzuki, M., and Yamamoto, M., 2011, "Numerical Simulation of Sand Erosion Phenomena in a Single-Stage Axial Compressor," J. Fluid Sci. Technol., **6**(1), pp. 98–113.

[15] Ghenaiet, A., 2012, "Study of Sand Particle Trajectories and Erosion Into the First Compression Stage of a Turbofan," ASME J. Turbomach., **134**(5), p. 051025.

[16] Zuniga, V., and Osvaldo, M., 2007, "Analysis of Gas Turbine Compressor Fouling and Washing on Line," Ph.D. thesis, Cranfield University, UK.

[17] Parker, G. J., and Lee, P., 1972, "Studies of the Deposition of Sub-Micron Particles on Turbine Blades," Proc. Inst. Mech. Eng., **186**(1), pp. 519–526.

[18] Elrod, C. E., and Bettner, J. L., 1983, "Experimental Verification of an Endwall Boundary Layer Prediction Method," Report No. AGRAD CP-351.

[19] Morini, M., Pinelli, M., Spina, P. R., and Venturini, M., 2010, "Computational Fluid Dynamics Simulation of Fouling on Axial Compressor Stages," ASME J. Eng. Gas Turbines Power, **132**(7), p. 072401.

[20] Reid, L., and Moore, R. D., 1978, "Design and Overall Performance of Four Highly-Loaded, High-Speed Inlet Stages for an Advanced High-Pressure-Ratio Core Compressor," NASA Report No. TP 1337.

[21] ANSYS FLUENT, 2010, Release 13.0.

[22] Morsi, S. A., and Alexander, A. J., 1972, "An Investigation of Particle Trajectories in Two-Phase Flow Systems," J. Fluid Mech., **55**(2), pp. 193–208.

[23] Clift, R., Grace, J. R., and Weber, M. E., 1978, "Bubbles, Drops, and Particles," Technical Report No. ■, Academic.

[24] Wang, T., and Dhanasekaran, T. S., 2008, "Calibration of CFD Model for Mist/Steam Impinging Jets Cooling," ASME Paper No. GT2008-50737.

[25] Tomas, J., 2006, "Mechanics of Particle Adhesion," [Extended Master Version of *Particles on Surfaces 8: Detection, Adhesion and Removal*, VSP Utrecht (2003)], pp. 183–229.

[26] Meher-Homji, C. B., Chaker, M., and Bromley, A. F., 2009, "The Fouling of Axial Flow Compressor—Causes, Effects, Susceptibility, and Sensitivity," ASME Paper No. GT2009-59239.

[27] Ahlert, K., 1994, "Effects of Particle Impingiment Angle and Surface Wetting on Solid Particle Erosion of AISI 1018 Steel," M.S. thesis, Department of Mechanical Engineering, The University of Tulsa, Tulsa, OK.

[28] Forder, A., Thew, M., and Harrison, D., 1998, "A Numerical Investigation of Solid Particle Erosion Experienced Within Oilfield Control Valves," Wear, **216**(2), pp. 184–193.

[29] Tian, T., and Ahmadi, G., 2006, "Particle Deposition in Turbulent Duct Flows—Comparisons of Different Model Predictions," J. Aerosol Sci., **38**(4), pp. 377–397.

[30] Suman, A., Morini, M., Kurz, R., Aldi, N., Brun, K., Pinelli, M., and Spina, P. R., 2014, "Quantitative CFD Analyses of Particle Deposition on a Transonic Axial Compressor Blade, Part II: Impact Kinematics and Particle Sticking Analysis," ASME Paper No. GT2014-25473. AQ8

[31] Silingardi, A., Astrua, P., Piola, S., and Ventrucci, I., 2013, "A Method for a Reliable Prediction of Heavy Duty Gas Turbines Performance Degradation due to Compressor Aging Employing Field Test Data," Power Gen Europe, Messe, Wien, Austria.